HHS Public Access

Author manuscript

Environ Sci Technol. Author manuscript; available in PMC 2019 July 17.

Published in final edited form as:

Environ Sci Technol. 2018 July 17; 52(14): 7745–7753. doi:10.1021/acs.est.8b02348.

Adsorption of PFOA at the Air-Water Interface during Transport in Unsaturated Porous Media

Ying Lyu[1,3], **Mark L Brusseau**[3], **Wei Chen**[3], **Ni Yan**[3], **Xiaori Fu**[3], and **Xueyu Lin**[1,2]

[1]Institute of Water Resources and Environment, Jilin University, Changchun, 130026, P.R. China

[2]College of Construction Engineering, Jilin University, Changchun, 130026, P.R. China

[3]Soil, Water and Environmental Science Department, Hydrology and Atmospheric Sciences Department, School of Earth and Environmental Sciences, 429 Shantz Bldg, University of Arizona

Abstract

Miscible-displacement experiments are conducted with perfluorooctanoic acid (PFOA) to determine the contribution of adsorption at the air-water interface to retention during transport in water-unsaturated porous media.. Column experiments were conducted with two sands of different diameter; at different PFOA input concentrations, water saturations, and pore-water velocities to evaluate the impact of system variables on retardation. The breakthrough curves for unsaturated conditions exhibited greater retardation than those obtained for saturated conditions, demonstrating the significant impact of air-water interfacial adsorption on PFOA retention. Retardation was greater for lower water saturations and smaller grain diameter, consistent with the impact of system conditions on the magnitude of air-water interfacial area in porous media. Retardation was greater for lower input concentrations of PFOA for a given water saturation, consistent with the nonlinear nature of surfactant fluid-fluid interfacial adsorption. Retardation factors predicted using independently determined parameter values compared very well to the measured values. The results showed that adsorption at the air-water interface is a significant source of retention for PFOA, contributing approximately 50 to 75% of total retention, for the test systems. The significant magnitude of air-water interfacial adsorption measured in this work has ramifications for accurate determination of PFAS migration potential in vadose zones.

Graphical Abstract

Correspondence to: Mark L Brusseau.

Supporting Information. Four additional figures are supplied as Supporting Information.

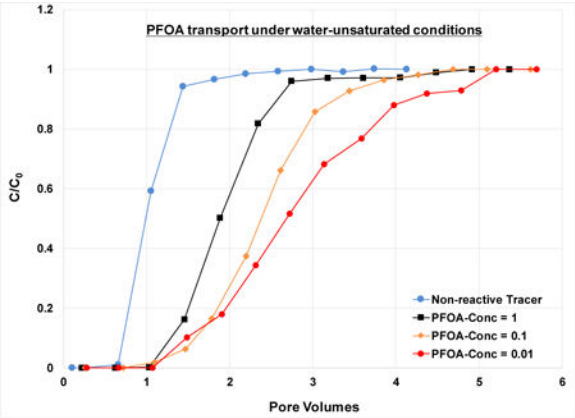

Keywords

Perfluoroalkyl; PFAS; retardation; partitioning; air-water interfacial adsorption

1. Introduction

The use of per- and poly-fluoroalkyl substances (PFAS) in numerous industrial, commercial, and military applications has resulted in their widespread distribution in the environment (cf., 1–4). Numerous reports have demonstrated the presence of PFAS in soil and groundwater at fire-fighting training sites, manufacturing sites, and airports (1,2,4–9). Perfluorooctanesulfonic acid (PFOS) and perfluorooctanoic acid (PFOA) are two primary PFAS of concern. The PFOS and PFOA concentrations observed at many of these sites exceed the lifetime health advisory of 0.07 μg/L (combined total) that was recently issued for long-term exposures to PFOA and PFOS through drinking water (10).

The risk posed by PFAS contaminated sites, as well as the effective remediation of such sites, is mediated by the transport and fate behavior of PFAS in the subsurface. Sorption of PFAS by the solid phase of geologic media is one phase-distribution retention process that can have significant impact on PFAS transport and attenuation. The sorption behavior of PFAS in geomedia has been investigated in several studies conducted over the past decade (e.g., 11–24). There exist however additional retention processes that need to be evaluated for their potential significance to PFAS retention and transport in the subsurface (24).

Recent detailed assessments of PFAS occurrence and fate at field sites have demonstrated that vadose-zone sources are a primary subsurface reservoir of PFAS, serving as long-term contaminant sources to groundwater (25–27). Hence, it is critical to examine the retention and transport behavior of PFAS in water-unsaturated porous media. One primary retention process for unsaturated systems is adsorption at the air-water interface. Several investigations have demonstrated its significance for retarding the transport of both non-surfactant (28–32) and surfactant constituents (e.g., 33–41). PFOS, PFOA, and related PFAS are surfactants and will accumulate at air-water interfaces. Research conducted for chemical and water-treatment applications has illustrated the strong air-water interfacial activity of PFOS and PFOA (e.g., 42–48). Thus, it is anticipated that adsorption to air-water interfaces

may be a significant retention mechanism for transport of select PFAS in the vadose zone (24). However, to our knowledge, the specific impact of air-water interfacial adsorption on PFAS transport in unsaturated porous media has not yet been investigated experimentally.

The objective of this research is to conduct an initial investigation of the contribution of adsorption at the air-water interface to PFAS retention during transport in water-unsaturated porous media. PFOA is selected as the representative PFAS, and experiments are conducted with two natural sands of different particle diameter. Column experiments are conducted at different PFOA input concentrations, water saturations, and pore-water velocities to evaluate the impact of system variables on retardation and transport of PFOA. Independent measurements of air-water interfacial retention variables are used to determine predicted retardation factors, which are then compared to the measured values. Surface-tension data collected from the literature for a homologous series of perfluorocarboxylates are used to calculate air-water interfacial adsorption coefficients to investigate their dependency on chain length.

Materials and Methods

Materials

PFOA (CAS#335–67-1) of 98% purity was purchased from AIKE Reagent (China). Sodium perfluorooctanoate (CAS#335–95-5) was also used in surface tension comparisons. Sodium chloride (NaCl, 0.01 M) was used as the background electrolyte solution for all surface-tension and miscible-displacement experiments. Solutions were prepared using distilled, deionized water. PFOA input concentrations (C_0) of 0.01, 0.1, and 1 mg/L were used for the miscible-displacement experiments. The 1 mg/L concentration represents the upper range of PFOA concentrations reported for groundwater, with for example, a value of >6 mg/L reported for Fallon NAS (6).

The surface tension of aqueous PFOA solutions (with 0.01 M NaCl) was measured using a De Nouy ring tensionmeter (Fisherscientific, Surface Tensiomat 21) following standard methods (ASTM D1331– 89). The tensiometer was calibrated with a weight of known mass. Each sample was measured three times with the deviation between measurements less than 0.7%. Two separate sets of measurements were conducted at different dates. In addition, a third set of measurements was conducted using a Kino automatic surface tensionmat employing the Wilhelmy plate method. Each sample was measured three times with the deviation between measurements less than 0.3%. Surface tension was also measured for Na-PFOA in DI water using the De Nouy ring tensiometer.

Surface-tension data for a C6-C11 homologous series of sodium perfluoroalkyl carboxylates were reported by Lunkenheimer et al. (45). Analysis of these data, shown in Figure S1 of Supporting Information (SI), provides an opportunity to determine K_{ai} values for a series of PFAS. These data are used to evaluate the influence of chain length on air-water adsorption potential. Surface-tension data for PFOS were reported by Vecitis et al. (43). These data are used to determine a K_{ai} value for comparison to the perfluoroalkyl carboxylate data.

Two porous media were used for the miscible-displacement experiments. The first is a 16/18 mesh natural quartz sand ranging in size from 1.0 to 1.3 mm with mean diameter of 1.2 mm. The second is a 40/50 mesh natural quartz sand with mean diameter of 0.35 mm. These media, which are anticipated to exhibit ideal and relatively low magnitudes of solid-phase adsorption, were selected specifically to focus on the impact of air-water interfacial adsorption.

The columns used in this study were constructed of acrylic to minimize interaction with PFOA, and were 15 cm long with inner diameter of 2.0 cm. Flow distributors were placed in contact with the porous media on the top and at the bottom of the column to help promote uniform fluid distribution and to support the media. Peristaltic pumps (BT100–02, Baoding Qili Precision Pump Co., Ltd, China) were used to provide fluid flow. As noted below, analysis of background samples collected from the column effluent revealed the absence of any interferences associated with the column or apparatus for PFOA determination.

Methods

The miscible-displacement experiments were conducted using methods we have used previously in numerous prior studies (e.g., 28,38,40). These methods have been demonstrated to produce steady-state water flow and uniform distributions of water saturation for unsaturated conditions (cf., Brusseau et al. (38)). For each experiment, the column was packed with air-dried sand to a uniform bulk density. The column was then saturated with aqueous solution and weighed to determine porosity. Column dead volume was measured to determine the effective resident pore volume of the sand pack. The columns were oriented vertically for all experiments. All experiments were conducted at room temperature (25±1ºC).

Preliminary tests were conducted with a nonreactive tracer solution (pentafluorobenzoic acid) to ensure that the columns were packed well and to characterize hydrodynamic conditions. Experiments were conducted with PFOA under saturated conditions to determine the impact of solid-phase adsorption on retardation and transport. Experiments were then conducted under unsaturated conditions to determine the additional impact of air-water interfacial adsorption. Nonreactive tracer tests were conducted at each selected water saturation.

Two pumps were connected to the system for the unsaturated flow experiments, one to each end of the column. To prepare for an unsaturated-flow experiment, the water-saturated column was first partially drained to the target water content. Differential rates of solution injection and extraction results in a change in water saturation under controlled conditions. Electrolyte solution was injected at a specified flow rate to the top of the column while the pump connected to the bottom end was used to withdraw solution at a higher flow rate. Once the target water saturation was achieved (as determined by monitoring column mass), the two pumps were set to the same flow rate. This setup produced constant flow rates, as determined by weighing each effluent sample (mean coefficient of variation, COV, = 4%). Experiments were conducted at three different water saturations for each sand.

Additional experiments were conducted for the 0.35 mm sand to examine the impact of system conditions on retardation. Most experiments were conducted at flow rates equivalent to mean pore-water velocities of ~30 cm/h. Experiments were also conducted at 17, 69, and 137 cm/hr to test for potential impacts of rate-limited mass transfer. Conditions for all experiments are presented in Table 1.

Samples of column effluent were collected in polypropylene tubes and analyzed immediately after collection. PFOA was analyzed by high-performance liquid chromatography (Agilent Model 1100, USA) and tandem mass spectrometry (TSQ quantum, Thermo Scientific, USA), i.e., LC-MS/MS. The column was an Agilent C18 maintained at 40 ºC. The dual mobile phase comprised 5 mM ammonium acetate and acetonitrile applied in a 60:40 gradient at a flow rate of 0.2 mL/min. The aqueous samples were injected directly, with injection volumes of 2 μL. Retention time was consistently ~4.3 min. MS/MS conditions were as follows: ionization mode: ESI-; capillary temperature: 300 ºC; nebulizer temperature: 300 ºC. Standard QA/QC protocols were employed. Blanks, background samples, and check standards were analyzed periodically for each sample set. The results for the first two were lower than the quantifiable detection limit. The calibration curve attained a coefficient of determination (r^2) larger than 0.999. The quantifiable detection limit was ~0.5 ug/L. Background aqueous samples collected from the column effluent before injection of PFOA revealed no measurable PFOA concentrations or other interferences for all experiments.

Data Analysis

Measured retardation factors were determined for each miscible-displacement experiment by the standard method of calculating the area above the breakthrough curve. Their uncertainty is very small (total uncertainty for the measured Rs are <2%), related to uncertainty in concentration and flow rate, which is small for these controlled experiments. These retardation factors incorporate the contributions of all relevant retention processes influencing transport. The retardation factor for aqueous-phase transport of solute undergoing retention by solid-phase adsorption and air-water interfacial adsorption is given as (34–38):

$$R = 1 + K_d\rho_b/\theta_w + K_{ai}A_{ai}/\theta_w \quad 1$$

where K_d is the solid-phase adsorption coefficient (cm^3/g), K_{ai} is the air-water interface adsorption coefficient (cm^3/cm^2), A_{ai} is the specific air-water interfacial area (cm^2/cm^3), ρ_b is porous-medium bulk density (g/cm^3), and θ_w is volumetric water content (volume of water per volume of porous medium, -). By phase balance, $\theta_w + \theta_a = n$, where θ_a is volumetric air content (−) and n is porosity. Water saturation is defined as $S_w = \theta_w/n$. The fraction of the measured total retention associated with adsorption at the air-water interface is determined as:

$$F_{AWIA} = \left[(R-1) - \left(K_d\rho_b/\theta_w\right)\right]/[R-1] \quad 2$$

Measured K_{ai} values are determined from the miscible-displacement experiments by rearranging equation 1, with R obtained from analysis of the breakthrough curve and all other variables determined independently.

The air-water interface adsorption coefficient, K_{ai}, can also be determined from the surface tension function (e.g., 34–38). The surface excess Γ (mol/cm^2) is related to aqueous phase concentration (C) using the Gibbs equation (e.g., 34,35,37):

$$\Gamma = \frac{-1}{\mathrm{RT}} \frac{\partial \gamma}{\partial\, lnC} = K_i C \quad 3$$

$$K_i = \frac{\Gamma}{C} = \frac{-1}{\mathrm{RTC}} \frac{\partial \gamma}{\partial\, lnC} \quad 4$$

where K_i represents the interfacial adsorption coefficient (in our case K_{ai}, cm), γ is the interfacial tension (dyn/cm), C represents the aqueous phase concentration (mol/cm^3), and R is the gas constant (erg/mol °K). The surface-tension data (Figure 1) were analyzed using methods described previously to obtain K_{ai} (34–38). This involves determining the local slope of the $\partial\gamma/\partial$lnC function at the selected solute concentration and applying equation 4. In this case, 1 mg/L is used to match the highest C_0 used in the miscible-displacement experiments. Determination of K_{ai} is problematic for significantly lower concentrations due to insensitivity of the surface-tension function at those concentrations. K_{ai} values determined from the surface-tension data will be compared to those determined from the transport experiments. K_{ai} values were also determined from the surface-tension data reported for the C6-C11 perfluoroalkyl carboxylate homologues and for PFOS to conduct a comparative analysis of molecular-structure effects.

Predicted retardation factors were calculated to compare to the measured values determined from the miscible-displacement experiments. Predicted values were determined using equation 1 as follows. Bulk density, porosity, and water content are known for each experiment. Measured K_d values are known from the column experiments conducted under saturated flow. Independent measurements of air-water interfacial area for 0.35-mm sand were obtained in prior experiments conducted using the standard aqueous interfacial partitioning tracer test method (40). However, measured values are not necessarily available for each specific water saturation employed for the PFOA experiments. A_{ai} values can be estimated for any specific water saturation using the following:

$$\mathrm{A_{ai}} = \left(1 - \mathrm{S_w}\right)\mathrm{A_{max}} \quad 5$$

where A_{max} is the maximum specific air-water interfacial area, determined or extrapolated at vanishing small S_w (e.g., 49). An A_{max} value of 216 (±17) is determined for the 0.35-mm sand from the data presented in Brusseau et al. (40). The robustness of this value is supported by the observation that very similar A_{max} values have been reported for ~0.35-mm

silica sand using different measurement methods, including surfactant mass-balance (A_{max} = 210, Schaefer et al., 37), gas-phase interfacial partitioning tracer (A_{max} = 200, Sung et al., 50), and dual-surfactant aqueous interfacial partitioning tracer (A_{max} = 217, Brusseau et al., 40) methods. No data are available for the 1.2-mm sand. Hence, an empirical correlation based on measured air-water interfacial area data reported in the literature was used to provide an estimated A_{max} value. The following equation was obtained: $A_{max} = 61.3d^{-1.2}$ (n = 7, r^2 = 0.97), where d is median grain diameter, using reported data for silica sands (35,37,38,40,50). An A_{max} of 50 cm^{-1} is obtained for the 1.2-mm sand using the regression.

Results and Discussion

Surface Tensions

The surface tension data for PFOA are presented in Figure 1. Very good consistency is observed among the three sets of measurements, conducted at different times using two different methods. The CMC occurs at approximately 4200 mg/L (~0.01 mol/L), with an associated surface tension of ~14 dyne/cm). These values are consistent with those reported in the literature (42,43). Analysis of the surface-tension data produced a K_{ai} value of 0.002 (±0.0005) cm for PFOA in the 0.01 M NaCl background electrolyte solution. The surface tensions for the sodium perfluoroalkyl carboxylate C6-C11 homologues are shown in Figure S1 of the SI. It is observed that the surface-tension data measured in this work for Na-PFOA matches very well with the literature data sets.

Transport and Retardation

Transport of the nonreactive tracer was ideal for saturated-flow conditions, with sharp arrival and elution waves (minimal spreading), and retardation factors of 1 (see Figure S2 in SI for the 0.35-mm sand). A simulated curve produced using the ideal advection-dispersion equation matches the measured breakthrough curve (BTC) quite well. The Peclet Number obtained for the simulation is 65, which corresponds to a longitudinal dispersivity of 0.2 cm. This very small value is consistent with the ideal transport behavior observed for the nonreactive tracer. Breakthrough curves for unsaturated-flow conditions exhibit slight additional spreading, as would be expected for unsaturated conditions. However, this is relatively insignificant, as the breakthrough curves exhibit generally ideal behavior overall. The results obtained for the nonreactive tracer tests indicate that the columns were well-packed and that water flow was uniform, with no significant preferential flow or presence of no-flow domains.

The breakthrough curves for PFOA transport in the 0.35 and 1.2 mm sands are presented in Figures 2 and 3, respectively, for selected experiments. The BTCs for the saturated-flow experiments are relatively sharp and symmetrical, consistent with the results of the nonreactive tracer tests. K_d values of 0.08 and 0.015 are determined from these experiments for the 0.35 and 1.2 mm sands, respectively (Table 1). These relatively small magnitudes are to be expected given the nature of the porous media used, silica sand with very low organic-carbon and metal-oxide contents, and no clay minerals.

The BTCs for the unsaturated-flow experiments are shifted noticeably to the right of the saturated-flow BTC for the 0.35-mm sand, indicating greater retardation (Figure 2). For example, the retardation factor is 2.0 for a saturation of 0.68, compared to 1.29 for the saturated conditions (Table 1). Similar results are observed to a lesser degree for the 1.2-mm sand (Figure 3). Retardation is observed to increase progressively for smaller PFOA input concentrations for the 0.35-mm sand (Figure 4), with retardation factors increasing from 2.0 to 2.4 to 2.8 (Table 1). The greater retardation observed for unsaturated conditions is attributable to the impact of adsorption at the air-water interface. These results are consistent with those obtained for transport of a hydrocarbon surfactant, sodium dodecylbenzenesulfonate, under unsaturated conditions (34,38,40).

Reasonable reproducibility for unsaturated-flow experiments is exhibited for the 0.35-sand (experiments 1–3), with a resultant COV of 2.4% for the retardation factor. Monitoring of the masses of the effluent samples revealed low temporal variability (COV=4%) and no significant differences in flow rate before and after arrival of the PFOA BTC. This indicates that there was no measurable surfactant-induced drainage for these experiments. This is consistent with expectations, given the use of low PFOA concentrations with respect to the surface-tension function, which produced at most ~3% reduction in surface tension.

Measured retardation factors for all experiments are reported in Table 1. Retardation increased with decreasing water saturation for both media. This is consistent with the standard behavior of unsaturated porous media wherein total (capillary + film) air-water interfacial area increases continuously with decreasing saturation, as has been demonstrated in numerous experimental and modeling studies (e.g., 34–38,51–58).

Inspection of Table 1 shows that retardation factors are lower for the larger diameter sand. For example, the mean value for the 0.35-mm sand is 2.0 for S_w = 0.68, compared to 1.23 for the 1.2-mm sand at S_w=0.65. This behavior is consistent with the impact of grain size on the magnitude of air-water interface, wherein larger-diameter media comprise smaller interfacial areas at equivalent water saturations (e.g., 35,49,55,57,59–61). It also reflects the smaller magnitude of solid-phase adsorption for the larger-diameter sand.

As noted, PFOA retardation was greater for lower input concentrations, with retardation factors increasing from 2.0 to 2.4 to 2.8 for C_0s of 1, 0.1, and 0.01 mg/L, respectively (experiments 10–12 in Table 1). This is consistent with the nonlinear nature of surfactant fluid-fluid interfacial adsorption. The corresponding measured K_{ai} values determined from the retardation factors are 0.0021, 0.0027, and 0.004 cm for C_0s of 1, 0.1, and 0.01 mg/L, respectively. To our knowledge, these represent the first such values for a PFAS measured under transport conditions. The K_{ai} value determined from the C_0=1 mg/L miscible-displacement experiment is essentially identical to the value determined from the PFOA surface-tension data (K_{ai} = 0.002 cm). This indicates that use of surface-tension data to determine K_{ai} values is an effective approach for PFAS, consistent with prior observations for hydrocarbon surfactants. Combining the K_{ai} values from miscible-displacement and surface-tension data provides a means to examine the concentration dependency of K_{ai}, as presented in Figure S3. It is observed that K_{ai} values decrease as concentrations increase, consistent with nonlinear adsorption behavior.

The fraction of total retention associated with air-water interfacial adsorption can be determined by subtracting the contribution of solid-phase adsorption from the total measured retention (eq. 2). The results show that adsorption at the air-water interface is a significant source of retention for PFOA, contributing approximately 50 to 75% of total retention (Table 1). This is consistent with the results of prior research conducted for transport of hydrocarbon surfactants and other contaminants in unsaturated media (28,29,30,32,38,39).

Prediction of Retardation

As discussed in the Methods section, PFOA retardation factors can be predicted for the unsaturated conditions using eq. 1 because values are known for all variables. Predicted retardation factors are presented in Table 1 for the C_0 = 1 mg/L experiments only, given the uncertainty associated with using surface-tension data for K_{ai} determination at very low concentrations. Note that the values in parentheses represent the 95% confidence intervals for combined error propagation for uncertainty in K_{ai} and A_{ai} values. The predicted values are statistically identical to the measured retardation factors for four of the five 0.35-mm sand experiments conducted under standard conditions (experiments 1–5), and very close for the fifth. They are also statistically identical for the 1.2-mm sand for the two higher water saturations (experiments 1–2). The concordance of predicted and measured values demonstrates that the impact of air-water interfacial adsorption is predictable as well as quantifiable for this system. In addition, it indicates that both air-water interfacial adsorption and solid-phase adsorption can be treated as effectively instantaneous processes under the extant conditions.

The impact of pore-water velocity was evaluated by conducting three experiments with velocities 0.5, 2, and 4.5 times larger than the standard velocity (experiments 7, 8, and 9 in Table 1). The measured retardation factor for the experiment conducted with a mean pore-water velocity half of the standard velocity is very similar to the measured R for the standard velocity (compare experiments 5 and 9) for similar water saturation. In addition, as noted above, it is observed that the predicted R values are similar to the measured R values for all standard-condition experiments. These results indicate that both solid-phase adsorption and air-water interfacial adsorption can be treated as essentially instantaneous under these conditions. It should also be noted that the mean pore-water velocities for the standard-condition unsaturated-flow experiments are larger than the velocity for the saturated-flow experiments (see Table 1). Thus, the significantly greater retardation observed for the unsaturated-flow experiments cannot be due to differential preferential-flow or rate-limited mass-transfer conditions between the saturated and unsaturated systems.

The measured retardation factors are somewhat smaller than the predicted values for the two experiments conducted at the fastest pore-water velocities (experiments 7 and 8). This may indicate that solid-phase adsorption and/or mass transfer to the air-water interface became rate-limited under the reduced residence times associated with the larger pore-water velocities. In addition, it is possible that interface mobility became an issue at the higher pore-water velocities, which would result in a reduced impact of interfacial adsorption on retardation (52).

The measured retardation factor is smaller than predicted for the 1.2-mm sand experiment conducted at the lowest water saturation of 0.35 (experiment 3). The BTC for this experiment exhibits greater spreading than the BTCs obtained for higher water saturations (Figures 2 and 3). This is indicative of the impact of disconnected flow paths associated with the relatively low water content. Under such conditions, the injected aqueous PFOA solution likely does not contact all of the air-water interface present, effectively reducing the magnitude of air-water interfacial retention. Such behavior has been observed for transport of hydrocarbon surfactant at low water saturations (e.g., 38,52).

Influence of Chain Length & QSPR Analysis

It has long been recognized that the surface activity of hydrocarbon surfactants is a function of chain length. This behavior has also been observed for PFAS (e.g., 45,46,48). For example, Lunkenheimer et al. (45) determined standard free energies of interfacial adsorption from surface-tension data measured for a homologous series of sodium perfluoro-n-alkanoates (data reproduced in Figure S1), and demonstrated a strong correlation of the energies to chain length. Hence, it is to be expected that the magnitude of the air-water interfacial adsorption coefficient would also correlate to chain length. The surface-tension data in Figure S1 were analyzed herein to determine K_{ai} values. As depicted in Figure 5, an excellent linear relationship exists between log K_{ai} and chain length.

The linear log K_{ai}-chain length relationship translates to a nonlinear relationship between log retardation factor and chain length (Figure 5). It is observed that, for this series of PFAS and extant conditions, retardation factors are appreciably greater than 1 only for chain lengths of 8 and greater. Retardation factors in the 100s are projected for the longer-chain homologues.

Correlations to chain length are generally accurate only for a given homologous series. For example, the log K_{ai} value for PFOS does not fall on the regression line (Figure 5). An effective way to account for differences in molecular structure is to use quantitative structure–property relationship (QSPR) analysis. QSPR is routinely used to examine correlations between properties such as aqueous solubility and molecular properties. Brusseau and colleagues, for example, used QSAR to analyze the influence of molecular structure on solid-phase sorption by geomedia (62,63). Bhhatarai and Gramatica conducted an extensive QSPR analysis for PFAS (64). They showed that aqueous solubility, vapor pressure, and CMC (critical micelle concentration) were all well described by simple QSPR models.

QSPR analysis is applied to the K_{ai} data reported in Figure 5 for the homologous series and for PFOS. Excellent correlation of log K_{ai} to the molecular descriptor ^3X is observed (Figure 6). This particular descriptor characterizes molecular connectivity and branching. It is of note that the data point for PFOS is well described by the correlation obtained for the perfluoroalkyl carboxylates. This correlation provides a means to estimate K_{ai} values for different PFAS.

Implications

Current published conceptual and mathematical models of PFAS transport and fate in the subsurface focus on solid-phase adsorption as the sole source of retardation. For example, all three of the recent detailed assessments of field-scale PFAS fate cited above employed this assumption. In addition, this assumption is used in recent comprehensive reports on PFAS management (65,66). The results of the research reported herein demonstrate that adsorption at the air-water interface can be a significant source of retention and retardation for PFAS transport in unsaturated porous media. Hence, retention and retardation in vadose-zone source areas may be substantially greater than what is typically estimated. This has significant ramifications for example for accurate determination of the migration potential of PFAS in vadose-zone sources and the magnitude of mass flux to groundwater. In addition, calculations of contaminant mass residing in vadose zones based on aqueous-concentration measurements would also be influenced by the existence of this additional retention process, with the potential for appreciable underestimation. Both of these elements have implications for risk assessment and remedial-action decision-making.

The results of the present study indicate that air-water interface adsorption should be considered when assessing PFAS transport and fate in the subsurface. The porous media used for this work were specifically selected to minimize the contribution of solid-phase sorption to retardation so as to focus on air-water interfacial adsorption. As demonstrated herein, the relative contribution of air-water interfacial adsorption to overall PFAS retardation will depend on the properties of the specific PFAS and its concentration, properties of the geomedia (magnitude of potential interfacial area, solid-phase adsorption potential), and system conditions (water saturation).

Supplementary Material

Refer to Web version on PubMed Central for supplementary material.

Acknowledgements

This work was supported by the NIEHS Superfund Research Program (grant# P42 ES04940). The authors thank the reviewers of the original and revised versions of the manuscript for their constructive comments.

References

1. Rayne S and Forest K, 2009 Perfluoroalkyl sulfonic and carboxylic acids: A critical review of physicochemical properties, levels and patterns in waters and wastewaters, and treatment methods. J. Environ. Sci. Health Part A 44, 1145–1199.
2. Ahrens L 2011 Polyfluoroalkyl compounds in the aquatic environment: a review of their occurrence and fate. J. Environ. Monit. 13: 20–31. [PubMed: 21031178]
3. Krafft MP and Riess JG. 2015 Per- and polyfluorinated substances (PFAS): environmental challenges. Curr. Opin. Colloid Interface Sci, 20, 192–212.
4. Cousins IT, Vestergren R, Wang Z, Scheringer M, and McLachlan MS 2016 The precautionary principle and chemicals management: The example of perfluoroalkyl acids in groundwater. Environ. Inter, 94, 331–340.
5. Moody CA; Field JA 2000 Perfluorinated surfactants and the environmental implications of their use in fire-fighting foams. Environ. Sci. Technol, 34: 3864–3870.

6. Moody CA; Field JA 1999 Determination of perfluorocarboxylates in groundwater impacted by fire-fighting activity. Environ. Sci. Technol, 33: 2800–2806.
7. Environmental Protection Agency (USEPA), 2009 Long-Chain Perfluorinated Chemicals (PFCs) Action Plan. 12 30, 2009, U.S. Environmental Protection Agency, Washington, DC https://www.epa.gov/assessing-and-managing-chemicals-under-tsca/long-chain-perfluorinated-chemicals-pfcs-action-plan
8. Backe WJ, Day TC, and Field JA 2013 Zwitterionic, cationic, anionic fluorinated chemicals in AFFF formulations and groundwater from U.S. military bases by non-aqueous large-volume injection HPLC-MS/MS. Environmental Science & Technology, 47: 5226–5234. [PubMed: 23590254]
9. Anderson RH, Long GC, Porter RC, Anderson JK 2016 Occurrence of select perfluoroalkyl substances at U.S. Air Force aqueous film-forming foam release sites other than fire-training areas: Field-validation of critical fate and transport properties. Chemo. 150: 678–685.
10. Environmental Protection Agency (USEPA). 2016 FACT SHEET PFOA & PFOS Drinking Water Health Advisories. 11 2016 EPA 800-F-16–003. U.S. Environmental Protection Agency, Washington, DC.
11. Liu JX and Lee LS 2005. Solubility and sorption by soils of 8:2 fluorotelomer alcohol in water and cosolvent systems. Environ. Sci. Technol. 2005, 39, 7535–7540. [PubMed: 16245825]
12. Liu J and Lee LS 2007 Effect of fluorotelomer alcohol chain length on aqueous solubility and sorption by soils. Environ. Sci. Technol, 41(15), 5357–5362. [PubMed: 17822102]
13. Higgins CP, and Luthy RG 2006 Sorption of perfluorinated surfactants on sediments. Environ. Sci. Technol. 40, 7251. [PubMed: 17180974]
14. Higgins CP, and Luthy RG 2007 Modeling sorption of anionic surfactants onto sediment materials: An a priori approach for perfluoroalkyl surfactants and linear alkylbenzene sulfonates. Environ. Sci. Technol. 41, 3254–3261. [PubMed: 17539534]
15. Johnson RL, Anschutz AJ, Smolen JM, Simcik MF, and Penn RL. 2007 The adsorption of perfluorooctane sulfonate onto sand, clay, and iron oxide surfaces. Journal of Chemical & Engineering Data 52: 1165–1170.
16. Carmosini N and Lee LS 2008 Partitioning of fluorotelomer alcohols to octanol and different sources of dissolved organic carbon. Environ. Sci. Technol, 42(17), 6559–6565. [PubMed: 18800530]
17. Chen H, Chen S, Quan X, Zhao YZ, and Zhao HM 2009 Sorption of perfluorooctane sulfonate (PFOS) on oil and oil-derived black carbon: Influence of solution pH and [Ca2+]. Chemo. 77: 1406–1411.
18. Pan G, Jia CX, Zhao DY, You C, Chen H, and Jiang GB 2009 Effect of cationic and anionic surfactants on the sorption and desorption of perfluorooctane sulfonate (PFOS) on natural sediments. Environ. Pollut. 157: 325–330. [PubMed: 18722698]
19. Ferrey ML, Wilson JT, Adair C, Su C, Fine DD, Liu X, and Washington JW 2012 Behavior and fate of PFOA and PFOS in sandy aquifer sediment. Groundwater Monit. Remed, 32(4), 63–71.
20. Guelfo JL and Higgins CP 2013 Subsurface transport potential of perfluoroalkyl acids at aqueous film-forming foam (AFFF)-impacted sites. Environ. Sci. Technol. 47: 4164–4171. [PubMed: 23566120]
21. Zhao L, Bian J, Zhang Y, Zhu L, and Liu Z 2014 Comparison of the sorption behaviors and mechanisms of perfluorosulfonates and perfluorocarboxylic acids on three kinds of clay minerals. Chemo. 114, 51–60.
22. Milinovic J, Lacorte S, Vidal M, Rigol A 2015 Sorption behaviour of perfluoroalkyl substances in soils. Sci. Total Environ. 511: 63–71. [PubMed: 25531590]
23. Hellsing MS, Josefsson S, Hughes AV, Ahrens L. 2016 Sorption of perfluoroalkyl substances to two types of minerals. Chemosphere, 159, pp. 385–391. [PubMed: 27323291]
24. Brusseau ML 2018 Assessing the potential contributions of additional retention processes to PFAS retardation in the subsurface. Science Total Environ. 613–614, 176–185.
25. Shin HM, Vieira VM, Ryan PB, Detwiler R, Sanders B, Steenland K, Bartell SM, 2011 Environmental fate and transport modeling for perfluorooctanoic acid emitted from the

Washington works facility in West Virginia. Environ. Sci. Technol. 45 (4), 1435–1442. [PubMed: 21226527]

26. Xiao F, Simcik MF, Halbach TR, Gulliver JS. 2015, Perfluorooctane sulfonate (PFOS) and perfluorooctanoate (PFOA) in soils and groundwater of a U.S. metropolitan area: Migration and implications for human exposure. Water Res, 72, 64–74. [PubMed: 25455741]
27. Weber AK, Barber LB, LeBlanc DR, Sunderland EM, and Vecitis CD, 2017 Geochemical and hydrologic factors controlling subsurface transport of poly- and perfluoroalkyl substances, Cape Cod, Massachusetts. Environ. Sci. Technol. 2017, 51, 4269–4279. [PubMed: 28285525]
28. Brusseau ML, Popovicova J, and Silva J 1997 Characterizing gas-water interfacial and bulk-water partitioning for transport of gas-phase contaminants in unsaturated porous media. Env. Sci. Technol, 31: 1645–1649.
29. Kim H, Rao PSC, Annable MD, 1998 Influence of air-water interfacial adsorption and gas-phase partitioning on the transport of organic chemicals in unsaturated porous media. Env. Sci. Technol, 32, 1253–1259.
30. Kim H, Annable MD, Rao PSC 2001 Gaseous transport of volatile organic chemicals in unsaturated porous media: effect of water-partitioning and air-water interfacial adsorption. Env. Sci. Technol, 35, 4457–4462. [PubMed: 11757601]
31. Costanza M and Brusseau ML 2000 Influence of adsorption at the air-water interface on the transport of volatile contaminants in unsaturated porous media. Env. Sci. Technol, 34: 1–11.
32. Costanza-Robinson MS, Carlson TD, Brusseau ML 2013 Vapor-phase transport of trichloroethene in an intermediate-scale vadose-zone system: retention processes and tracer-based prediction. J. Contam. Hydrol, 145: 182–189.
33. Karkare MV and Fort T, 1996 Determination of the air-water interfacial area in wet “unsaturated” porous media. Langmuir 12, 2041–4044.
34. Kim H, Rao PSC, Annable MD, 1997 Determination of effective air–water interfacial area in partially saturated porous media using surfactant adsorption. Water Resour. Res, 33 (12), 2705–2711.
35. Anwar AHMF, Bettahar M, Matsubayashi UJ, 2000 A method for determining air–water interfacial area in variably saturated porous media. J. Contam. Hydrol, 43, 129–146.
36. Anwar AHMF, 2001 Experimental determination of air–water interfacial area in unsaturated sand medium. New Approaches Characterizing Groundwater Flow. In: Proceedings. of XXXI IAH Congress, Munich, Germany, September 10–14, Vol. 2, pp. 821–825.
37. Schaefer CE, DiCarlo DA, Blunt MJ, 2000 Experimental measurement of air–water interfacial area during gravity drainage and secondary imbibition in porous media. Water Resour. Res. 36, 885–890.
38. Brusseau ML, Peng S, Schnaar G, and Murao A 2007 Measuring air-water interfacial areas with x-ray microtomography and interfacial partitioning tracer tests. Env. Sci. Technol, 41: 1956–1961. [PubMed: 17410790]
39. Brusseau ML, Janousek H, Murao A, and Schnaar G 2008 Synchrotron x-ray microtomography and interfacial partitioning tracer test measurements of NAPL-water interfacial areas. Water Resour. Res, Vol. 44, W01411, doi:10.1029/2006WR005517. [PubMed: 23678204]
40. Brusseau ML, El Ouni A, Araujo JB, and Zhong H 2015 Novel methods for measuring air-water interfacial area in unsaturated porous media. Chemo. 127: 208–213.
41. Zhong H, El Ouni A, Lin D, Wang B, and Brusseau ML 2016 The two-phase flow IPTT method for measurement of nonwetting-wetting liquid interfacial areas at higher nonwetting saturations in natural porous media, Water Resour. Res, 52: 5506–5515. [PubMed: 28959079]
42. Downes N, Ottewill GA, Ottewill RH 1995 An investigation of the behavior of ammonium perfluoro-octanoate at the air/water interface in the absence and presence of salts. Colloids and Surfaces A: Physicochemical and Engineering Aspects, 102: 203–211.
43. Vecitis CD, Park H, Cheng J, Mader BT, Hoffmann MR 2008 Enhancement of perfluorooctanoate (PFOA) and perfluorooctanesulfonate (PFOS) activity at acoustic cavitation bubble interfaces. Journal of Physical Chemistry 112: 16850–16857.

44. Meng P, Deng SB, Deng S, , Lu X, Du Z, Wang B, Huang J, Wang Y, Yu G, Xing B. 2014 Role of air bubbles overlooked in the adsorption of perfluorooctanesulfonate on hydrophobic carbonaceous adsorbents. Environ. Sci. Technol, 48, 13785–13792. [PubMed: 25365738]
45. Lunkenheimer K, Prescher D, Hirte R, Geggel K, 2015 Adsorption properties of surface chemically pure sodium perfluoro-n-alkanoates at the air/water interface: counterion effects within homologous series of 1:1 ionic surfactants. Langmuir 31, 970–981. [PubMed: 25540840]
46. Psillakis E, Cheng J, Hoffmann MR, Colussi AJ 2009 Enrichment factors of perfluoroalkyl oxoanions at the air/water interface. The Journal of Physical Chemistry A Letters, 113, 8826–8829.
47. López-Fontán JL, Sarmiento F, Schulz PC 2005 The aggregation of sodium perfluorooctanoate in water. Colloid Polym. Sci, 283, 862–871.
48. Hendricks JO 1953 Industrial fluoro-chemicals. Industrial Engin. Chem, 45, 99–105.
49. Brusseau ML, Narter M, Schnaar S and Marble J 2009 Measurement and estimation of organic-liquid/water interfacial areas for several natural porous media. Environmental Science & Technology, 43, 3619–3625.
50. Sung M and Chen B-H. 2011 Using aliphatic alcohols as gaseous tracers in determination of water contents and air–water interfacial areas in unsaturated sands. J. Contam. Hydrol. 126, 226–234. [PubMed: 22115088]
51. Cary JW, 1994 Estimating the surface area of fluid phase interfaces in porous media. J. Contam. Hydrol. 15, 243–248.
52. Kim H, Rao PSC, Annable MD 1999 Gaseous tracer technique for estimating air-water interfacial areas and interface mobility. Soil Sci. Soc. Am. J, 63, 1554–1560.
53. Or D and Tuller M 1999 Liquid retention and interfacial area in variably saturated porous media: Upscaling from single-pore to sample-scale model. Water Resour. Res, 35, 3591–3605.
54. Oostrom M; White MD; Brusseau ML 2001 Theoretical estimation of free and entrapped nonwetting-wetting fluid interfacial areas in porous media. Adv. Water Resour, 24, 887–898.
55. Costanza-Robinson MS and Brusseau ML 2002 Air-water interfacial areas in unsaturated soils: Evaluation of interfacial domains. Water Resour. Res, 38, 131–137.
56. Dalla E, Hilpert M, Miller CT Computation of the interfacial area for two fluid porous medium systems. J. Contam. Hydrol. 2002, 56, 25–48. [PubMed: 12076022]
57. Peng S and Brusseau ML 2005 Impact of soil texture on air-water interfacial areas in unsaturated sandy porous media. Water Resour. Res, Vol. 41, W03021, doi: 10.1029/2004WR003233.
58. Brusseau ML, Peng S, Schnaar G, and Costanza-Robinson MS 2006 Relationships among air-water interfacial area, capillary pressure, and water saturation for a sandy porous medium, Water Resour. Res, 42, W03501, doi:10.1029/2005WR004058.
59. Cho J and Annable MD 2005 Characterization of pore scale NAPL morphology in homogeneous sands as a function of grain size and NAPL dissolution. Chemo. 61, 899–908.
60. Dobson R, Schroth MH, Oostrom M, and Zeyer J 2006 Determination of NAPL-water interfacial areas in well-characterized porous media. Environ. Sci. Technol. 40, 815–822. [PubMed: 16509323]
61. Costanza-Robinson MS, Harrold KH, and Lieb-Lappen RM 2008 X-ray microtomography determination of air-water interfacial area-water saturation relationships in sandy porous media. Environ. Sci. Technol, 42, 2949–2956. [PubMed: 18497149]
62. Brusseau ML 1993 Using QSAR to evaluate phenomenological models for sorption of organic compounds by soil. Environ. Toxic. Chem, 12, 1835–1846.
63. Hu Q, Wang X, and Brusseau ML 1995 Quantitative structure-activity relationships for evaluating the influence of sorbate structure on sorption of organic compounds by soil. Environ. Toxic. Chem, 14, 1133–1140.
64. Bhhatarai B and Gramatica P 2011 Prediction of aqueous solubility, vapor pressure and critical micelle concentration for aquatic partitioning of perfluorinated chemicals. Environ. Sci. Technol, 45, 8120–8128. [PubMed: 20958003]
65. CONCAWE, 2017 Environmental fate and effects of poly and perfluoroalkyl substances (PFAS) Network for Industrially Contaminated Land in Europe, CONCAWE.

66. CRCCARE 2017. Assessment, management and remediation guidance for perfluorooctanesulfonate (PFOS) and perfluorooctanoic acid (PFOA) – Part 5: management and remediation of PFOS and PFOA, CRC CARE Technical Report no. 38, CRC for Contamination Assessment and Remediation of the Environment, Newcastle, Australia.

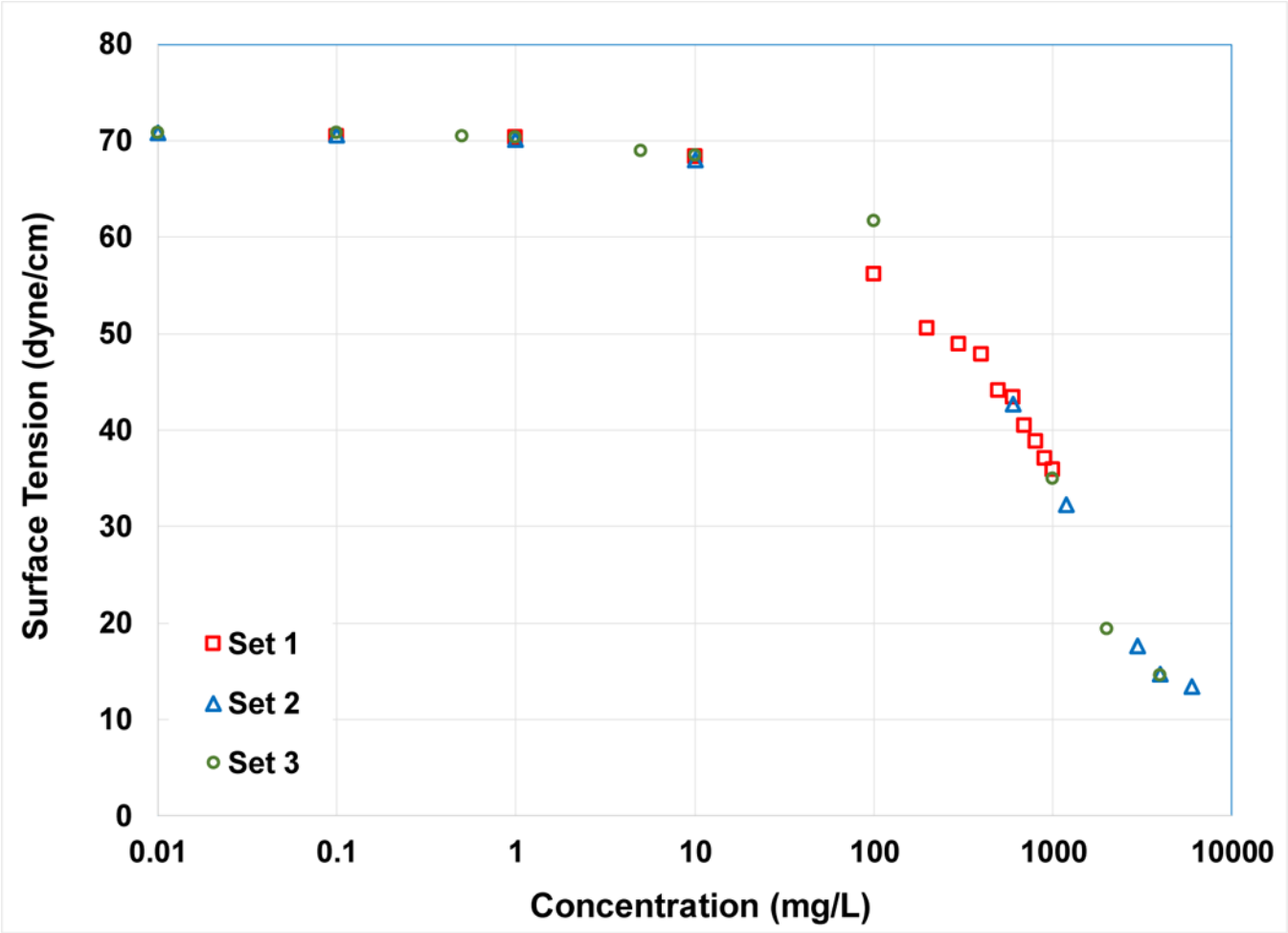

Figure 1.
Measured surface tension for PFOA in 0.01 M NaCl electrolyte solution.

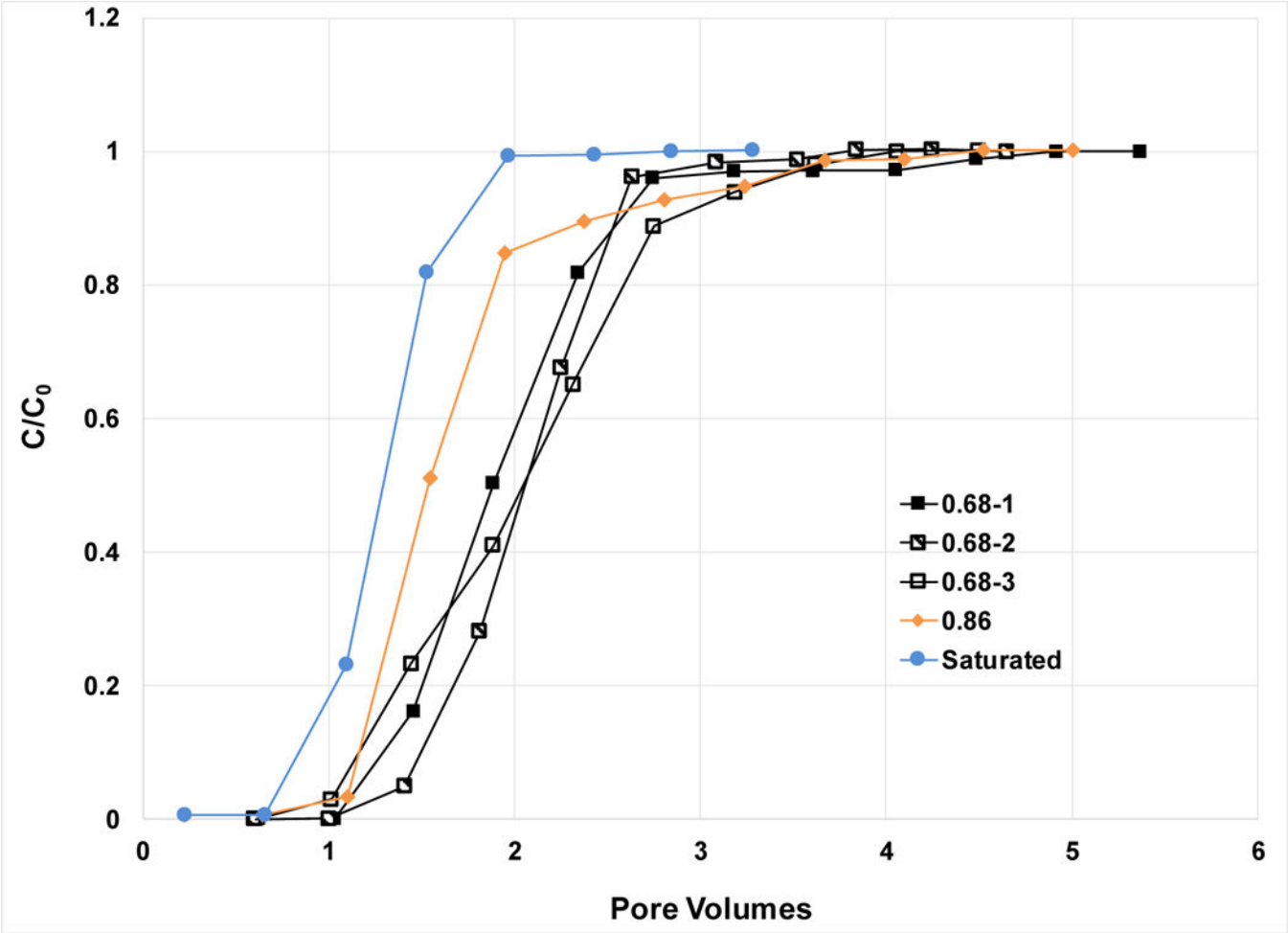

Figure 2.

Breakthrough curves for PFOA transport in the 0.35-mm sand; C_0 = 1 mg/L. Values in the legend refer to water saturation.

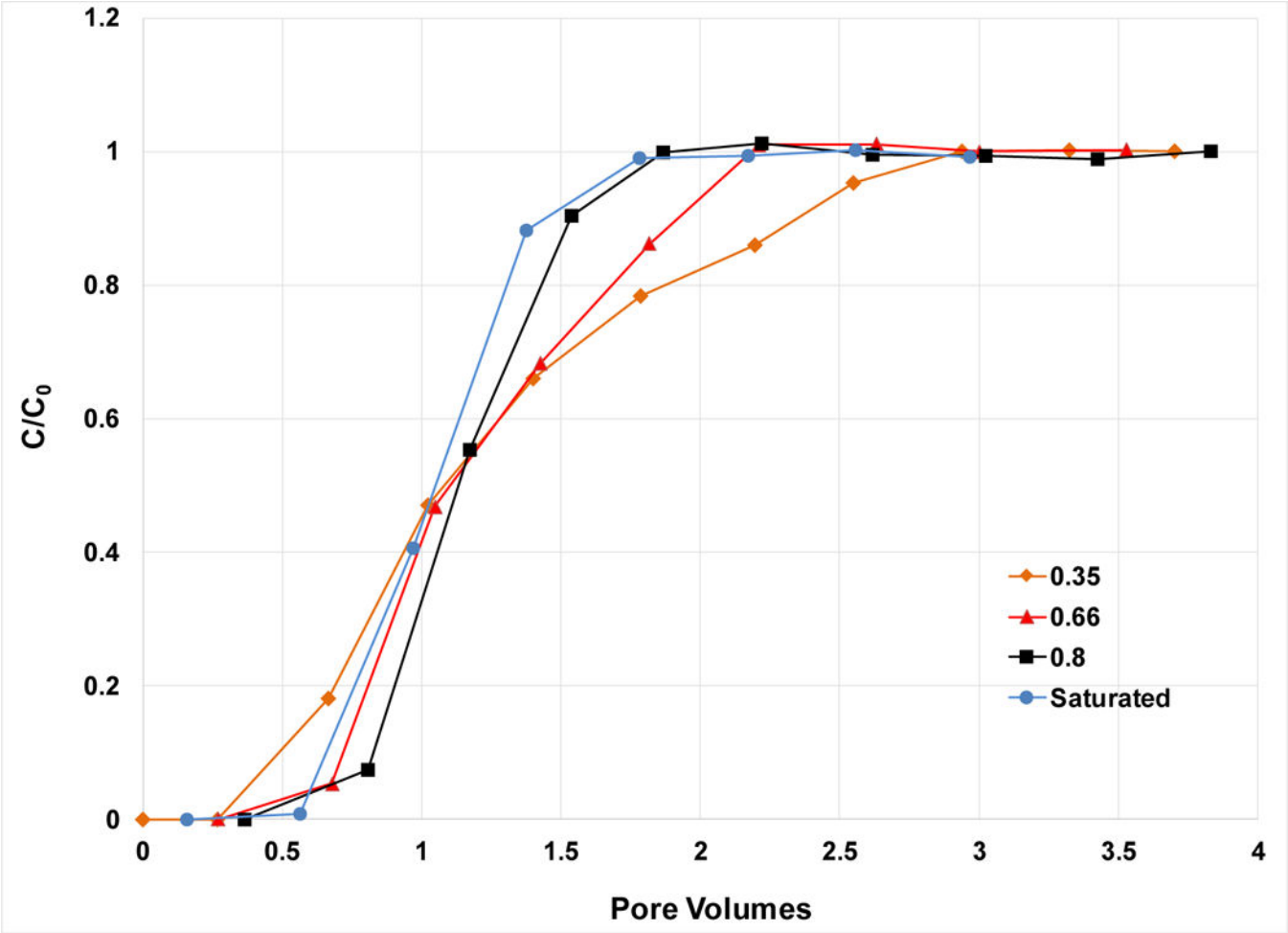

Figure 3.

Breakthrough curves for PFOA transport in the 1.2-mm sand; C_0 = 1 mg/L. Values in the legend refer to water saturation.

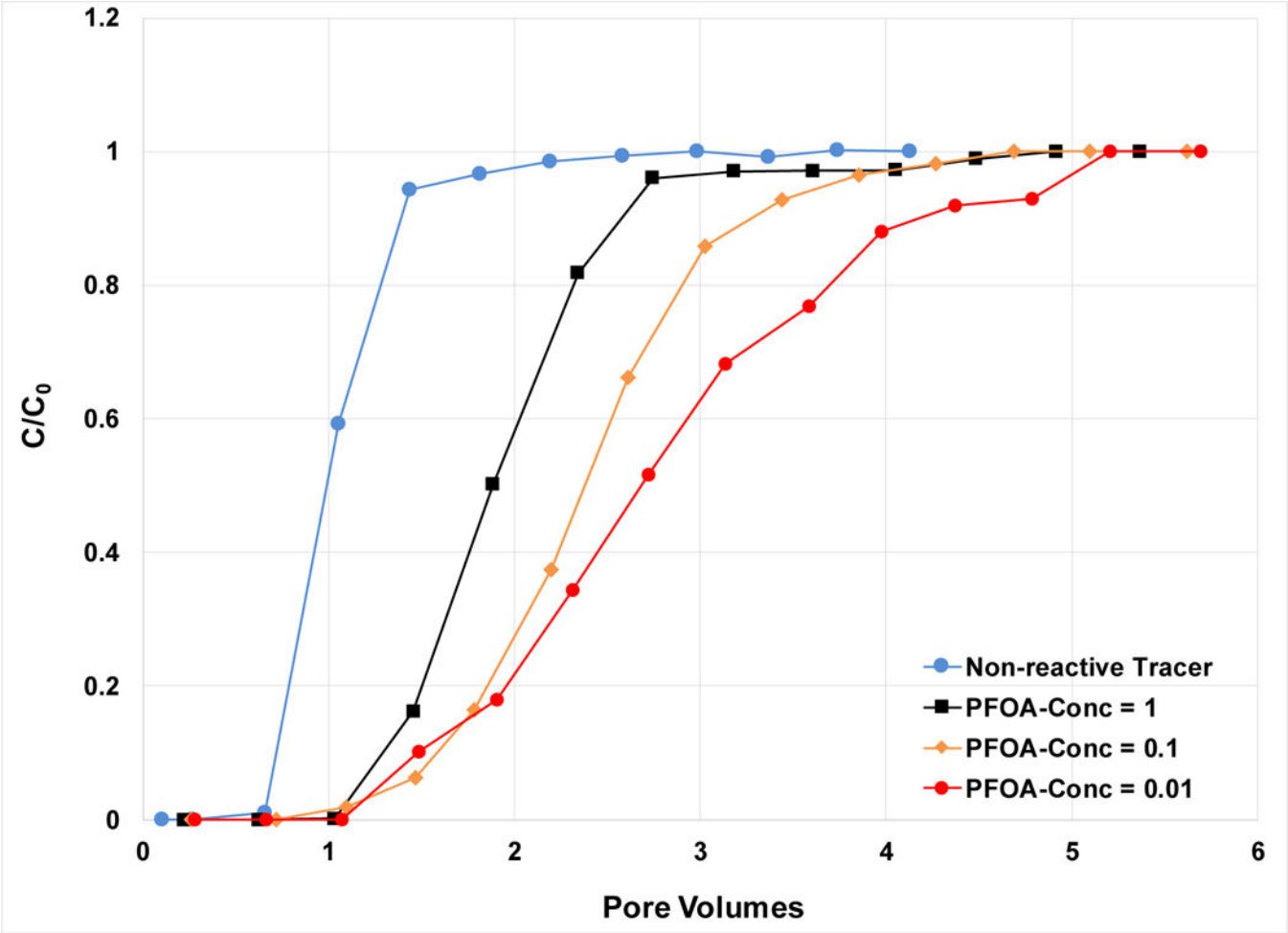

Figure 4.

Breakthrough curves for PFOA transport in the 0.35-mm sand for different input (C_0) concentrations. Water saturation is 0.68.

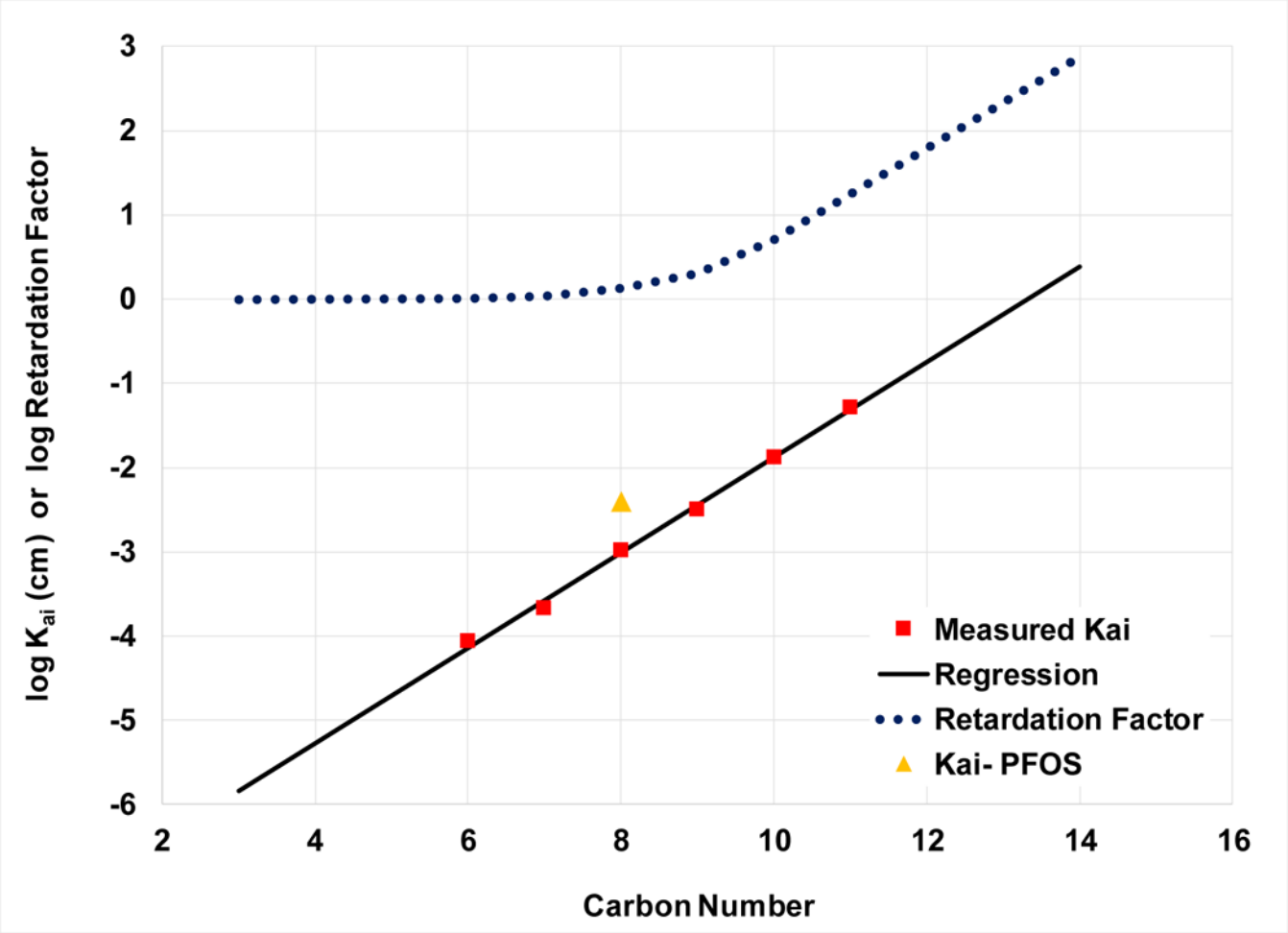

Figure 5.

Correlation of air-water adsorption coefficient (K_{ai}) and Retardation Factor (accounting solely for air-water adsorption) versus carbon chain length for a homologous series of sodium perfluoroalkyl carboxylates. A K_{ai} value for PFOS is included for comparison. K_{ai} values are calculated for [PFAS] = 1 mg/L. Representative values measured for the 0.35-mm sand are used to calculate R (θ_w = 0.23; A_{ia} = 73 cm^{-1}). Regression equation: log K_{ai} = 0.56 · Cn - 7.5, r^2 = 0.996.

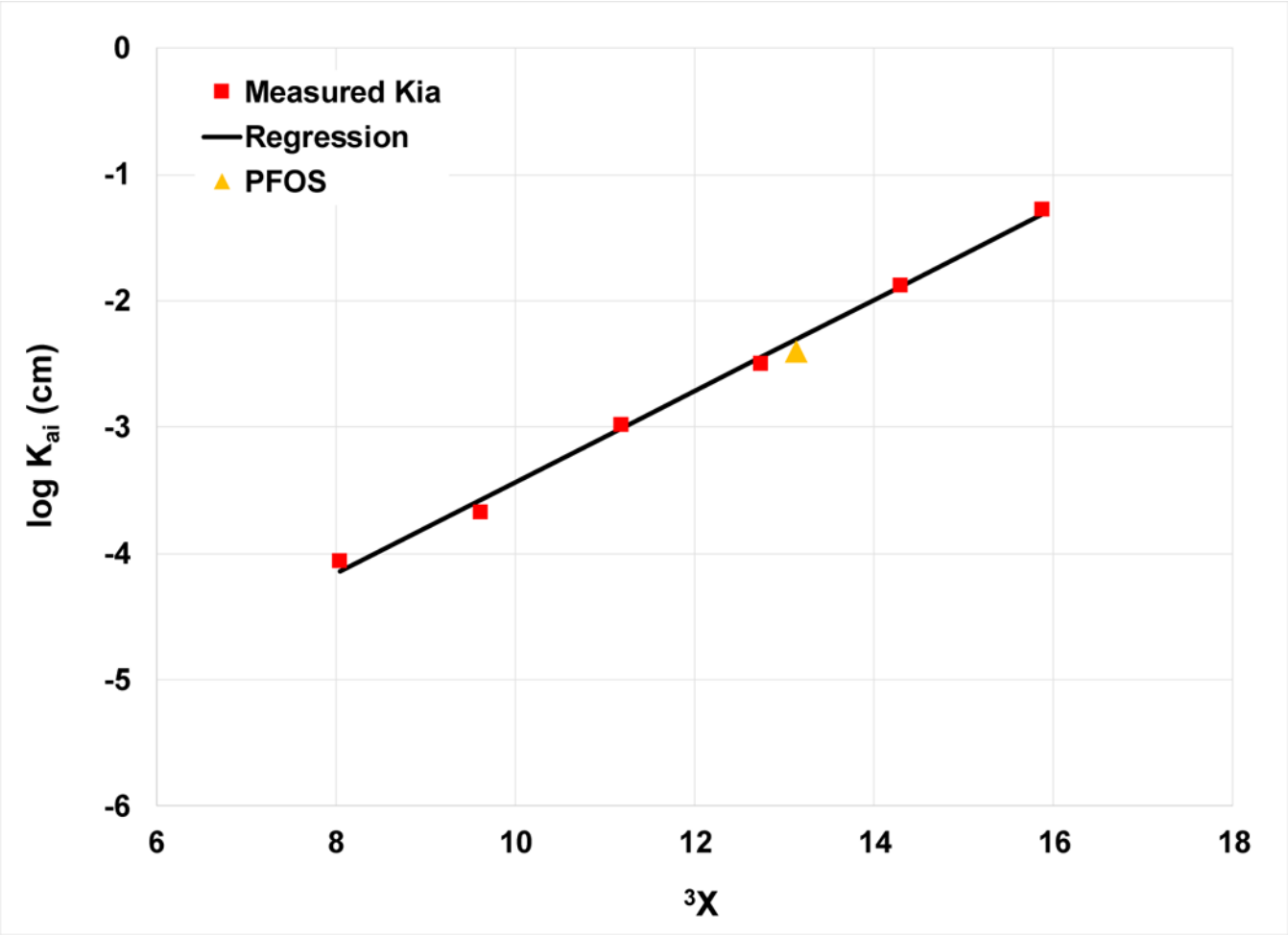

Figure 6.

QSPR analysis of log K_{ai} for a homologous series of sodium perfluoroalkyl carboxylates and for PFOS. Regression (not including PFOS): log $K_{ai} = 0.36 \cdot {}^{3}X - 7.1$, $r^2 = 0.996$. Values of ^{3}X reported in (64).

Table 1.

Measured and Predicted Retardation Factors.

Expt	Water Saturation	Measured R	F_{AWIA} [a]	Predicted R [b]	Notes
0.35-mm Sand					
Sat	1	1.29	-	-	v = 27 cm/h; K_d = 0.08
1	0.688	1.96	0.53	1.99 (1.83–2.18)	v = 37 cm/hr [e]
2	0.680	2.05	0.57	2.02 (1.85–2.22)	$\bar{R}_{1-3}$ [c] = 2.02 (1.96–2.07)
3	0.683	2.04	0.57	2.00 (1.83–2.20)	COV [d] = 2.4%
4	0.865	1.68	0.47	1.55 (1.49–1.61)	
5	0.760	1.85	0.52	1.78 (1.67–1.92)	
7	0.770	1.60	0.37	1.74 (1.65–1.88)	v = 69 cm/h
8	0.775	1.52	0.28	1.72 (1.62–1.85)	v = 137 cm/h
9	0.770	1.91	0.56	1.76 (1.65–1.88)	v = 17 cm/h
10	0.670	2.30	0.65	-	C_0 = 0.1 mg/L
11	0.680	2.41	0.68	-	C_0 = 0.1 mg/L
12	0.680	2.80	0.75	-	C_0 = 0.01 mg/L
1.2-mm Sand					
Sat	1	1.06	-	-	K_d = 0.015
1	0.800	1.16	0.55	1.14 (1.12–1.16)	
2	0.650	1.21	0.57	1.23 (1.18–1.28)	
3	0.350	1.26	0.36	1.64 (1.49–1.82)	

[a] F_{AWIA} = fraction of total retention associated with air-water interfacial adsorption

[b] 95% confidence interval in parentheses incorporating combined uncertainty in K_{ai} and A_{ai}

[c] Mean of experiments 1–3

[d] Coefficient of variation for experiments 1–3

[e] Mean pore-water velocity for all unsaturated-flow experiments except as noted.